Metallomics

Accepted Manuscript

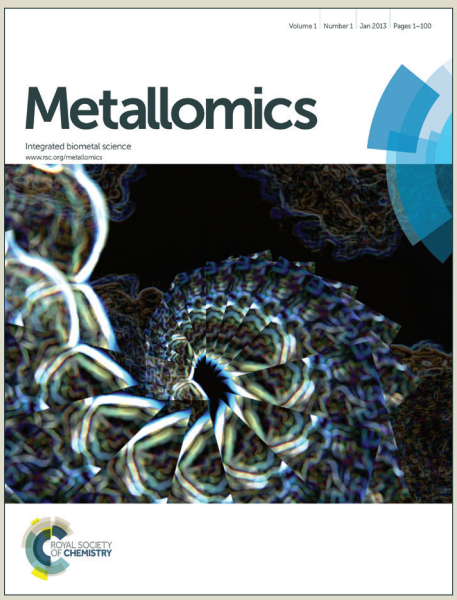

ROYAL SOCIETY OF CHEMISTRY

www.rsc.org/metallomics

Tumor microenvironment in focus: LA-ICP-MS bioimaging of a preclinical tumor model upon treatment with platinum(IV)-based anticancer agents

Sarah Theiner[1,2], Christoph Kornauth[3], Hristo P. Varbanov[1], Markus Galanski[1], Sushilla Van Schoonhoven[2,4], Petra Heffeter[2,4], Walter Berger[2,4], Alexander E. Egger[5*], Bernhard K. Keppler[1,2]

[1] Institute of Inorganic Chemistry, University of Vienna, Vienna, Austria

[2] Research Platform 'Translational Cancer Therapy Research', University of Vienna, Vienna, Austria

[3] Institute of Clinical Pathology, Medical University of Vienna, Vienna, Austria

[4] Institute of Cancer Research, Department of Medicine I and Comprehensive Cancer Center of the Medical University, Medical University of Vienna, Vienna, Austria

[5] ADSI – Austrian Drug Screening Institute GmbH, Innsbruck, Austria

[*]Corresponding author: Alexander E. Egger; ADSI-Austrian Drug Screening Institute GmbH, Innrain 66a, 6020-Innsbruck, Austria; alexander.egger@adsi.ac.at;

Tel.: +43(0)512-507-36305

Keywords: LA-ICP-MS, bioimaging, metal-based anticancer drugs, preclinical murine tumor model

Abstract

The selection of drug candidates for entering clinical development relies on *in vivo* testing in (solid) tumor animal models. However, the heterogeneity of tumor tissue (e.g. in terms of drug uptake or tissue composition) is rarely considered when testing novel drug candidates. Thus, we used the murine colon cancer CT-26 tumor model to study the spatially-resolved drug distribution in tumor tissue upon repetitive treatment of animals over two weeks with three investigational platinum(IV)-based anticancer agents, oxaliplatin or satraplatin. A quantitative laser-ablation-inductively coupled plasma-mass spectrometry (LA-ICP-MS) imaging method revealed a heterogeneous platinum distribution, which correlated well with histologic features of the tumor and surrounding tissue at microscopic level. In most of the cases, higher amounts of intratumoral platinum were found in the surrounding tissue than in the malignant parts of the sample. This indicates that determination of average platinum amounts (e.g. by microwave-assisted digestion of the sample followed by analysis with ICP-MS) might overestimate drug uptake in tumor tissue causing misleading conclusions.

In addition, we studied the platinum distribution in kidneys of treated animals to probe if accumulation in cortex and medulla predict potential nephrotoxicity. A 10-fold increase of platinum in the cortex of the kidney over the medulla was observed for oxaliplatin and satraplatin. Although these findings are similar to the platinum distribution of the nephrotoxic anticancer drug cisplatin, treatment with the compounds of our study did not show signs of nephrotoxicity in clinical use or clinical trials (oxaliplatin, satraplatin) and did not result in alteration of renal structures. Thus, predicting side effects based on bioimaging data by LA-ICP-MS should be considered with caution.

To the best of our knowledge, this is the first LA-ICP-MS study on spatially-resolved platinum accumulation in tissues after repetitive platinum-based anticancer drug treatment to mice bearing a preclinical tumor model.

Introduction

Chemotherapy for cancer treatment frequently includes one of the worldwide-approved platinum(II)-based compounds (cisplatin, carboplatin or oxaliplatin).[1] In the last decades, effort has been made to develop novel platinum(IV)-based cytostatics (e.g. tetraplatin, iproplatin and satraplatin) with focus on the reduction of side effects, overcoming the resistance occurring with platinum(II)-based drug treatment and improvement of oral bioavailability.[2-4] Platinum(IV) complexes can exert high kinetic inertness to substitution reactions, assuming their stability in the gastrointestinal tract (GIT) and in the blood stream.[5] A prerequisite for their anticancer activity is the formation of active platinum(II) species upon two-electron reduction preferably in the hypoxic tumor tissue (prodrug-concept).[6] Therefore, platinum(IV) complexes could be considered as an orally applicable, safe alternative over the established platinum(II)-based chemotherapeutics.[6,7] Satraplatin ((OC-6-43)-bis(acetato)amminedichlorido(cyclohexylamine)platinum(IV)) has been the first orally active platinum-based drug evaluated in clinical trials.[8] Despite positive results against refractory prostate cancer, after completion of clinical phase III trial, satraplatin was not approved by the FDA, as it failed to demonstrate decisive benefits with regard to the survival rate.[9,10]

To gain information on the *in vivo* properties of novel drugs, animal models are widely used to investigate their toxicological profile, pharmacokinetic behavior and therapeutic efficacy.[11-13] Based on these data, the most promising drug candidates are then selected for further (pre)clinical development. However, due to the enormous costs of clinical trials, additional information for the evaluation of novel drug candidates is of high interest, e.g. knowledge on the spatially-resolved (<100 µm) drug accumulation in the target tissue. In the case the compound of interest contains a non-physiological heteroatom (such as Pt), visualization thereof can be accomplished by micro-X-ray fluorescence (µ-XRF)[14] or laser ablation (LA) hyphenated to ICP-MS (LA-ICP-MS).[15-18] LA-ICP-MS combines fast sample preparation, visualization of elemental distributions independent from the chemical binding partner and

highly sensitive quantification in the sub µg/g order in thin tissue sections.[16,19] It has become of great interest in cancer research and diagnosis to detect tumor markers with the help of metal-labelled antibodies[20,21] and to identify possible protein binding partners of metallodrugs after 2D gel electrophoresis.[22,23] However, there are only few reports on the applications of LA-ICP-MS as imaging tool for metal-based anticancer agents in biological tissue samples. Herewith, the effect of cisplatin-treatment on mice kidneys, testis and cochlea[24-26] as well as platinum accumulation in tumor of rats after hyperthermic treatment with oxaliplatin have been investigated.[27] In addition, the quantitative platinum and ruthenium distribution of cisplatin and the investigational ruthenium complex NKP1339 in different tissues of mice has been compared using LA-ICP-MS.[28] Combined imaging techniques of LA-ICP-MS and matrix-assisted laser desorption/ionisation-mass spectrometry (MALDI-MS) have been applied to analyze patient samples from peritoneal carcinosis treated intraperitoneally with cisplatin or oxaliplatin.[29]

We have recently reported the *in vivo* anticancer activity of three novel platinum(IV)-based drug candidates in the colon cancer model CT-26 together with the average platinum levels in different mice tissues and serum upon treatment.[30,31] However, in these studies the impact of tumor heterogeneity (e.g. varying degrees of vascularization and necrotic areas) as well as drug distribution between malignant and adjacent benign tissue at microscopic level was not considered. Thus, within this paper we assessed the spatially-resolved platinum distribution of compound **1**-**3** (Figure 1) in tumor and kidney tissue in comparison with satraplatin and oxaliplatin by means of LA-ICP-MS. The obtained data were compared with histological evaluations as well as total platinum levels measured by ICP-MS. To the best of our knowledge, this is the first report on quantitative spatially-resolved platinum biodistribution by LA-ICP-MS in an *in vivo* tumor model upon treatment with platinum(IV)-based anticancer agents.

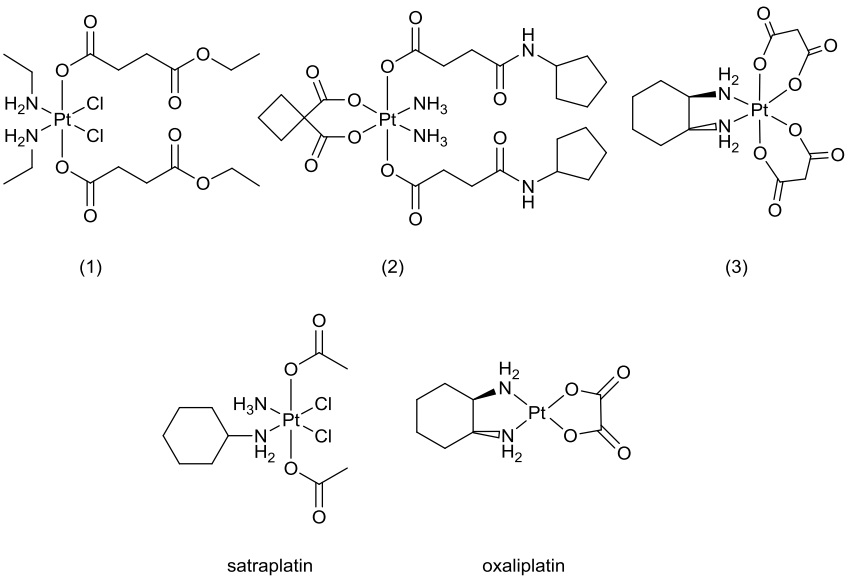

Figure 1. Structural formulas of platinum complexes under investigation; compound **1** ((OC-6-33)-dichloridobis((4-ethoxy)-4-oxobutanoato)bis(ethylamine)platinum(IV)), compound **2** ((OC-6-33)-diammine(cyclobutane-1,1-dicarboxylato)bis((4-cyclopentylamino)-4-oxobutanoato)platinum(IV)), compound **3** ((OC-6-22)-((1R,2R)-diaminocyclohexane)bis(malonato)platinum(IV)), satraplatin ((OC-6-43)-bis(acetato)amminedichlorido(cyclohexylamine)platinum(IV)) and oxaliplatin ((1R,2R)-cyclohexane-1,2-diamine)(ethanedioato-O,O')platinum(II).

Experimental

Chemicals

Synthesis and characterization of compound **1**, **2** and **3** was described previously.[31-33] Satraplatin was synthesized according to ref.[34]; oxaliplatin was prepared using standard literature methods as described in ref.[35] Milli-Q water (18.2 MΩ cm, Milli-Q Advantage, Darmstadt, Germany) was used for all dilutions for ICP-MS measurements. Nitric acid (≥65%, p.a., Fluka, Buchs, Switzerland) was further purified in a quartz sub-boiling point distillation unit (Milestone-MLS GmbH, Leutkirch, Germany) before usage. Platinum and rhenium standards for ICP-MS measurements were derived from CPI International (Amsterdam, The Netherlands). Tissue-Tek medium (Sakura Finetek, The Netherlands) was used for embedding of the cryosections. All other reagents and solvents were obtained from commercial sources and were used without further purification.

Animal experiments

Animal experiments were approved by the local ethics commission and carried out according to the Austrian and FELASA guidelines for animal care and protection. Six- to eight-week-old Balb/c mice were purchased from Harlan Laboratories (San Pietro al Natisone, Italy). The animals were kept in a pathogen-free environment and every procedure was done in a laminar airflow cabinet. Murine CT-26 cells (5×10^5) were injected subcutaneously into the right flank and therapy was started when tumor nodules were palpable (day 4). Mice were treated with the compounds at day 4, 7, 11, and 14 using the regimens summarized in Table S1. Animals were controlled for distress development every day and tumor size was assessed regularly by caliper measurement. Mice were anesthetized on day 15 approx. 24 h after the last drug application and organs were collected and stored at -20°C for quantitative platinum determination by solution-based ICP-MS. For LA-ICP-MS measurements, tumor and kidney

of one representative mouse was collected, immediately shock-frozen in liquid nitrogen and kept at -80°C until analysis.

Sample preparation for LA-ICP-MS, apoptosis counting and histological evaluation

For LA-ICP-MS measurements, tumor and kidney samples were embedded in Tissue-Tek medium and cryosectioned into slices of 20 µm thickness with a cryotom (Microm HM 550, Thermo Fischer). The cryosections were placed onto glass slides, air-dried and kept at room temperature until analysis. A consecutive cryoslice of 5 µm of the respective organ was stained with haematoxylin-eosin (H&E) using standard protocols. Histological evaluation was done with an Olympus BH2 standard light microscope. In addition, another part of the tumor/kidney was paraffin-embedded, sliced and H&E-stained by routine histological methods for apoptosis counting.

Microwave-assisted digestion of tissue samples and solution-based ICP-MS measurements

Digestion of tissue samples (approx. 10-30 mg) was performed with sub-boiled nitric acid using a microwave system Discover SP-D (CEM Microwave Technology, Germany). The following microwave parameters were used: temperature: 200°C; ramp time: 4 min; hold time: 6 min; maximal power: 300 W. Digested samples were diluted with Milli-Q water resulting in nitric acid concentrations lower than 3% and platinum concentrations lower than 20 ng/g. The total platinum content was determined with an ICP-quadrupole MS instrument Agilent 7500ce (Agilent Technologies, Waldbronn, Germany). The ICP-MS instrument was equipped with a CETAC ASX-520 autosampler (Nebraska, USA) and a MicroMist nebulizer at a sample uptake rate of approx. 0.25 ml/min. The instrument was tuned daily in order to achieve maximum sensitivity. Rhenium served as internal standard for platinum to account for instrumental fluctuations and matrix effects. The ICP-MS was equipped with nickel cones and

operated at an RF power of 1550 W. Argon was used as plasma gas (15 l/min) and as carrier gas with a flow rate of ~ 1.1 l/min. The dwell time was set to 0.1 s and the measurement was performed in 10 replicates. The Agilent MassHunter software package (Workstation Software, Version B.01.01, 2012) was used for data processing.

Quantitative bioimaging in tissue samples by LA-ICP-MS

Bioimaging with LA-ICP-MS, including quantification was performed according to a previously described procedure with slight modifications, using matrix-matched calibration standards.[28] For this purpose, commercially available pig liver was homogenized (homogenizer, Minilys, Peqlab, USA) and spiked with liquid platinum standards yielding platinum concentrations between 1-30 µg/g. The final platinum concentrations of the calibration standards were validated by ICP-MS measurements after microwave-assisted acid digestion using the same conditions as for the organs. Standards were run at the beginning and at the end of the laser experiment, and additionally in the middle when ablation time exceeded two hours in order to monitor instrumental drift.

A Nd:YAG solid state laser (NWR 213, ESI, Fremont, CA, USA) at a wavelength of 213 nm was used to obtain spatially-resolved distribution of platinum in tumor and kidney sections. The laser beam path was equipped with a square-shaped laser spot table ensuring a constant delivery of energy onto the moving sample throughout the entire diameter of the laser beam. An optical sample map of the region of interest was generated prior to the measurement. The output laser energy was tuned daily in order to ensure complete ablation of the sample material. Ablation was performed at 10 Hz using parallel line scans, a spot size of 70 µm, scan speed of 40 µm/s and spacing of 10 µm between the lines. The energy of the laser was increased to reach the substrate (=complete ablation) latest upon 10 shots (corresponding to a movement of the sample stage of approx. half the laser diameter). Assessment of complete ablation was evaluated upon termination of the sequence using an optical microscope.The

resulting sample energy was in the range of 0.13-0.16 mJ corresponding to a fluence between 2.7-3.2 J/cm². The ablated sample material was transferred to the ICP-MS instrument with helium (quality 5.0) at a flow rate of 400 ml/min. The warm-up time of the laser was set to 10 s and the wash out delay to 10 s. Laser ablation data was recorded using a Triple Quadrupole ICP-MS Agilent 8800 (Agilent Technologies, Tokyo, Japan) and processed with the Agilent MassHunter software package (Workstation Software, Version B.01.03, 2013). The instrumental parameters for LA-ICP-MS are given in Table 1. The software Igor Pro (Wavemetrics, Igor Pro 6.34A) together with its add-on Iolite (Iolite Version 2.5) was used for further data processing and generation of platinum distribution maps.[36] The data reduction scheme 'Trace_Elements' including blank subtraction and no smoothing of the visualization was applied according to the manual by the authors (Iolite User Manual, Version 2.0).[37] The aspect ratio of the image was set according to the dimensions of the ablated area in order to obtain accurately shaped pictures. In the case matrix-matched standards were measured for quantitative bioimaging, the platinum concentration of each standard was assigned in the scale bar of the image to the corresponding average counts. If not otherwise stated, the thresholds in the color bar were set to 0 and a platinum concentration of approx. 1.8 µg/g for all visualizations in order to facilitate comparison of the platinum amounts between the images solely by the color. In addition, the average platinum concentration (determined by ICP-MS after microwave-assisted digestion) in tissue originating from the same sample, is marked with an asterisk to prove the validity of the obtained quantitative imaging results (Figure 2).

Assessment of average platinum concentrations at microscopic level by means of LA-ICP-MS was based on a greyscale color scheme for image export in Iolite, providing a linear correlation between the grey value and the registered counts per second (CPS) of the isotope ^{195}Pt. The CPS were correlated with the concentration of the ablated standards enabling conversion of grey values to concentrations (expressed in µg/g) using ImageJ (Version

1.48v).[38] Upon calibration, the average platinum concentrations were read out using the histogram function of ImageJ.

Table 1. Instrumental parameters of LA-ICP-MS.

	LA-ICP-MS
RF power [W]	1350
Cone material	Nickel
Carrier gas [l/min]	1.10
Make up gas [l/min]	-
Plasma gas [l/min]	15
Monitored isotopes	^{195}Pt
Dwell time [s]	0.1
Number of replicates	1

Results and Discussion

Average platinum levels in tumor and kidney sections

The murine colon carcinoma CT-26 model was recently used to assess the *in vivo* anticancer activity and pharmacokinetics of compound **1**-**3** in comparison with satraplatin and oxaliplatin.[30,31] For this purpose, CT-26-bearing mice (n=4) were treated four times (on day 4, 7, 11, and 14) with the respective drugs. The dosages and routes of administration are summarized in detail in Table S1. Concentrations were chosen equimolar to satraplatin or equimolar to each other for better comparison of the platinum accumulation in tissue. In the case of compound **3**, the dose exhibiting activity on the leukemia model L1210 was administered,[31] whereas oxaliplatin-treated mice received the maximal tolerable dose.[39] Twenty-four hours after the last drug application, the mice were sacrificed and tissue samples were collected. The average platinum concentrations in tumor and several organs (including kidney, liver, lung; determined by ICP-MS) have recently been published[30,31] and are summarized in Table S1. Table 2 shows the average platinum levels of the tumor and kidney samples of the individuals used for the here presented study. In all cases, a representative animal was chosen for LA-ICP-MS bioimaging, which differed not more than 25% and 30% in case of tumor and renal platinum content, respectively, from the previously reported mean values. Consequently, in accordance to recently published data,[30,31] the rank of the platinum concentrations in tumor and kidney increased in the following order: compound **2** < satraplatin < oxaliplatin < compound **1** (i.p. and p.o.) < compound **3**.

In order to obtain quantitative information with LA-ICP-MS, matrix-matched standards (consisting of pig liver, spiked with liquid platinum standard solutions) were prepared for calibration.[28] The experimentally determined platinum concentrations of the standards were used to plot calibration curves yielding in all cases correlation coefficients > 0.99 (as example see Figure S1).

Table 2. Average platinum concentrations in tumor and kidney samples of the treated mouse selected for bioimaging by LA-ICP-MS. Values were determined by ICP-MS after microwave-assisted digestion and the results are given as mean ± standard deviation (samples from one mouse were measured in triplicates). In addition, the average concentration was determined by LA-ICP-MS using the histogram function of ImageJ as described in the experimental section.

compound	route of admin.	Pt admin. [µg/g]	Pt concentration [µg/g]		
			tumor (ICP-MS)	kidney (ICP-MS)	tumor (LA-ICP-MS)
satraplatin	p.o.	15.63	0.70 ± 0.06	2.37 ± 0.18	0.81
1	p.o.	15.63	1.66 ± 0.18	8.54 ± 0.45	0.90
1	i.p.	2.58	1.29 ± 0.24	8.15 ± 0.38	1.18
2	i.p.	2.58	0.72 ± 0.15	2.16 ± 0.56	0.66
3	i.p.	11.04	5.06 ± 0.14	12.78 ± 0.33	4.60
oxaliplatin	i.v.	4.42	0.96 ± 0.08	4.54 ± 0.17	1.15

Platinum distribution in tumor sections using LA-ICP-MS

The platinum distribution in the CT-26 tumors after treatment with the respective platinum compounds was determined at microscopic level by LA-ICP-MS (Figure 2) and correlated with the local tissue histology (visualized by H&E stain of a consecutive slide) as well as the previously determined average platinum content of the tumors. For the LA-ICP-MS experiments, the upper threshold of the intensity bars of all visualizations was scaled to platinum concentrations of ~1.8 µg/g, with the exception of compound **3** (Figure 2E) which was scaled to ~8.2 µg/g. In general, the LA-ICP-MS data were in good agreement with the average platinum content assessed previously by ICP-MS (indicated by an asterisk inserted into the color legend).

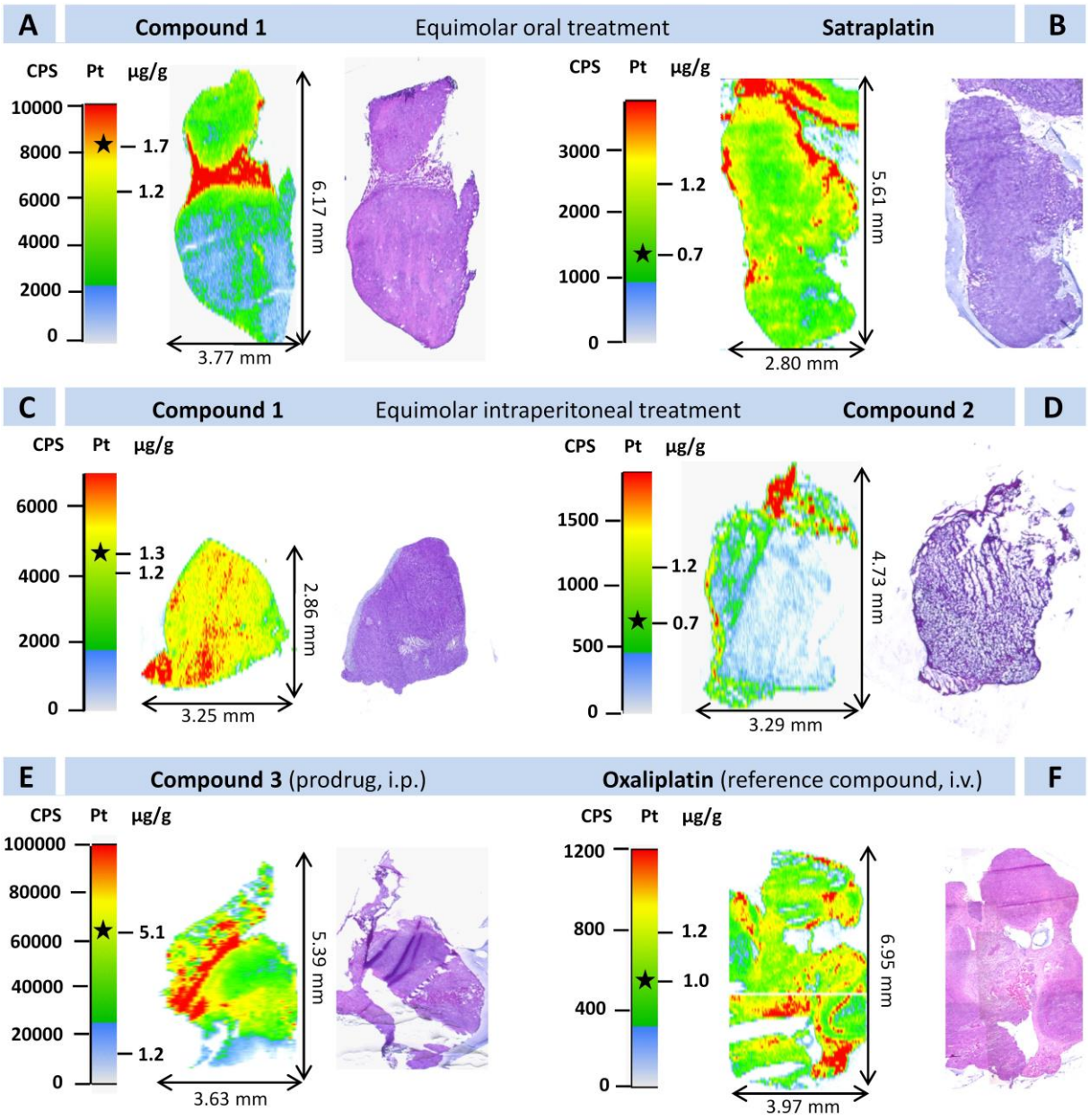

Figure 2. Platinum distribution in CT-26 tumor sections measured by LA-ICP-MS. Mice were treated with equimolar doses of (A) compound **1** (51.7 mg/kg, p.o.) or (B) satraplatin (40 mg/kg, p.o.), (C) compound **1** (8.5 mg/kg, i.p.) or (D) compound **2** (10 mg/kg, i.p.); with (E) compound **3** (30 mg/kg, i.p.) or (F) oxaliplatin (9 mg/kg, i.v.) on day 4, 7, 11, and 14. For LA-ICP-MS measurements cryosections were used. In addition, a consecutive H&E-stained cryosection is shown for comparison. The asterisks within the intensity bars correspond to the average platinum concentration determined by ICP-MS after microwave-assisted digestion.

The detailed measurements by LA-ICP-MS revealed that due to morphological heterogeneity of the tumor sections, the average platinum concentration and the spatially-resolved platinum

distribution pattern differed. Thus, although the majority of the ablated sample area exhibited a relatively homogeneous platinum distribution, also larger islets of increased platinum levels (indicated by red color) could be observed in all tumor sections. The following causes for this finding have to be considered: (1) artefacts resulting from the sample preparation (e.g. tissue compressions or duplicates) (2) heterogeneity of tumor tissue (e.g. due to varying degrees of necrosis/apoptosis, vascularization or susceptibility to the applied drug) (3) non-tumor tissue originating from the treated animal (e.g. connective tissue, muscle tissue). In order to further enlighten the nature of these regions, combined interpretation of grey-scaled images taken prior to ablation of the tissue samples and of H&E-stained consecutive tissue sections was conducted. In order to rule out artifacts, originating from different tissue types, ablation of ^{13}C was used as indication for varying degrees of organic matter. A representative ^{13}C image (compound **1**, corresponding to Figure 2A) showed a homogeneous distribution of organic matter over the whole tumor tissue (Figure S2).

In detail, compound **1** (dosed orally; Figure 2A) exhibited areas of platinum enrichment corresponding to loose soft tissue sparsely infiltrated by tumor cells and striated muscle from the treated mouse. The adjacent regions which accumulated platinum to lesser extent could be assigned to more solid areas of the tumor. According to the analysis by LA-ICP-MS, the tumor itself accumulated platinum in concentrations of approx. 0.5-1.2 µg/g, whereas loose soft tissue exhibited increased platinum levels of around 2.0-3.5 µg/g (Figure 3, top; dotted regions). The average platinum concentration of this sample was ~1.7 µg/g (Table 2), indicating that the platinum enrichment in the non-malignant tumor areas also distinctly affects quantitative measurements of total organ levels. The ablated sample after intraperitoneal administration of compound **1** (Figure 2C) revealed solely unstructured tumor tissue containing platinum levels of ~1.4 µg/g. This is in accordance with the average platinum concentration (~1.3 µg/g, Table 2) analyzed by ICP-MS. An overestimation of the tumor-specific platinum levels determined by ICP-MS was also found in other investigated

platinum(IV) samples. Compound **2** (Figure 2D and Figure S3, middle) exhibited a similar platinum accumulation profile as compound **1** after p.o. administration. Increased platinum amounts could be observed in areas of soft tissue with a lower density of infiltrating tumor cells, most probably corresponding to host tissue (approx. 0.7-1.5 µg/g) surrounding the tumor and lower, but relatively homogeneously distributed platinum levels in tumor tissue (~0.1-0.3 µg/g). The administered platinum amount upon intraperitoneal treatment with compound **3** was around 4.5-times higher than for compound **1** and **2**, which resulted in higher platinum accumulation in tumor (Figure 2E and Figure S3, bottom). The tissue section exhibited areas of distinctly different platinum amounts ranging from ~1.2 to ~8.2 µg/g. Most parts of the ablated sample area showed platinum concentrations between 4.5 and 5 µg/g, whereas also areas with elevated platinum levels of ~8 µg/g (indicated by red color) could be found.

For comparison, mice were treated orally with satraplatin (Figure 2B) and intravenously with oxaliplatin (Figure 2F) which corresponds to the respective clinically-relevant administration route. In contrast to the experimental compounds, increased platinum levels could not only be detected in areas of loose non-malignant soft tissue but also in some areas of tumor tissue (Figure 3, bottom and Figure S3, top). For satraplatin, these regions were found mainly at the edge of the tumor with platinum amounts of ~1.5-1.8 µg/g, whereas the rest of the tumor tissue exhibited platinum levels of ~0.7 µg/g. Treatment with oxaliplatin resulted in a relatively heterogeneous platinum distribution pattern with platinum concentrations ranging from ~0.8-1.5 µg/g. In these samples, the platinum enrichment (~1.0-1.5 µg/g) clearly correlated with tumor nodules composed of mitotically active, highly atypical cells as observed in H&E-stained tissue sections (Figure 3, bottom; dashed lines and Figure S4). Still, platinum was highly concentrated in soft tissue containing lower density of tumor cells.

In general, areas of (loose) soft tissue within and/or surrounding the tumor comprise increased amounts of platinum. The histologic nature of this tissue (e.g. microvessels or connective tissue) is matter of ongoing studies.

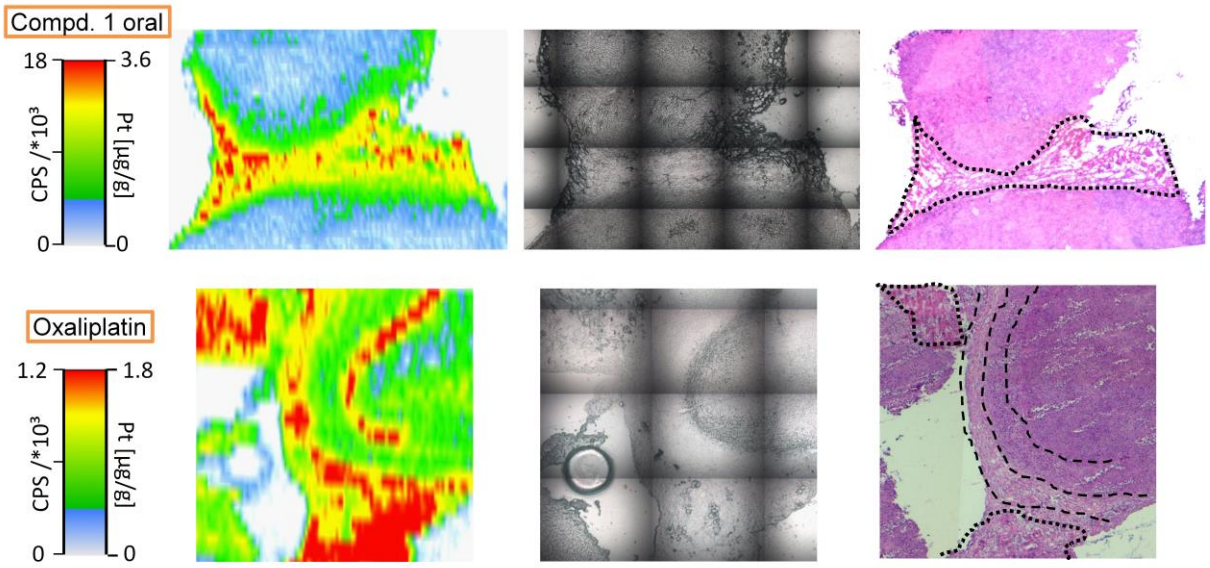

Figure 3. Detailed view of ablated tumor samples after treatment with compound **1** (p.o., top) and oxaliplatin (i.v., bottom); laser platinum image (left), sample map taken prior to laser ablation (middle) and H&E-stained section (right). The dotted spots in the H&E-stained slides correspond to loose connective tissue with sparsely scattered tumor cells. The dashed lines indicate areas of necrotic tissue within the tumor nodule.

As a next step, we addressed the question whether these differences in intratumoral drug distribution correlate with the anticancer activity of the tested platinum drugs. In addition to the previously published tumor growth throughout the experiment (time-span of two weeks),[30,31] the final tumor weight at day 15 is displayed in Figure S5. Based on the reported tumor growth kinetics, compound **2** and satraplatin were inactive under the experimental conditions used, while compound **1** (administered i.p. or p.o.) showed activity to some extent. On the other hand, oxaliplatin as well as compound **3** exhibited the highest activity of the investigated compounds. In the case of compound **3**, preliminary results of histological

evaluations indicated that this activity is based on both apoptosis induction as well as reduction of the mitotic cell population in the malignant tissue (Figure S6).

Equimolar dosages of satraplatin and compound **1** as well as of compound **1** and compound **2** (Table 2) were administered p.o. and i.p., respectively, which allows direct comparison of their spatially-resolved platinum distribution in tumor tissue.

In the case of compound **2** (Figure 2D), the comparison of the laser image with the histological stains showed that the platinum influx seemed to be restricted mainly to peritumoral (connective) tissue with elevated platinum levels of ~0.7-1.5 µg/g. In cancerous tissue only lower amounts of platinum (~0.1-0.3 µg/g) could be detected. These findings could be an explanation for the lack of anticancer activity of this compound on the CT-26 model. In contrast, compound **1** (Figure 2C) dosed equimolar to compound **2** (Figure 2D) deeply penetrates into the malignant tissue, probably explaining its activity. The third generation platinum(II)-based anticancer drug oxaliplatin is part of the standard therapeutic strategy against colon cancer in clinics and was therefore used as positive control in our study.[40, 41] In addition, we compared it with compound **3**, a platinum(IV) prodrug that is expected to form identical active metabolites like oxaliplatin.[31] Both compounds were active in the CT-26 tumor model and accumulated not only in soft tissue surrounding the tumor but also penetrated and accumulated in tumor tissue. However, due to varying dosages and routes of administration between oxaliplatin and compound **3**, their concentrations in tissue cannot be compared in our study. Our data show that LA-ICP-MS seems a promising tool to better investigate and understand the response of tumor models to metal-based anticancer drug treatment.

So far, only few reports have been published, dealing with metal-based anticancer drug uptake (cisplatin and oxaliplatin) in tumor tissue and their visualization by LA-ICP-MS.[27,29] Both studies aimed to investigate the treatment of peritoneal carcinosis by hyperthermic intraperitoneal chemotherapy. Thus, mass spectrometry was used to study the penetration

depth of the applied platinum-based drugs into tumor tissue of rat[27] or human samples[29] up to a treatment time of 60 min. In these investigations, the platinum influx was restricted mainly to the tumor periphery which is a logical consequence of the direct contact of the tumor tissue with the highly-concentrated perfusion solution.[27,29] In the here performed experiments, in contrast, drug transport to the tumor tissue has to be considered as exclusively via the blood stream, as it is the case for the vast majority of anticancer treatment regimens in clinics. Additionally, we applied repetitive treatments over a time-span of two weeks to gain deeper information on drug response in preclinical *in vivo* experiments. The extent of drug penetration into cancerous tissue in correlation with the anticancer activity can be of importance to estimate the potential of novel metal-based anticancer drug candidates, but cannot be assessed solely by microwave-assisted digestion and ICP-MS analysis. Spatially-resolved information on the platinum distribution revealed differences compared to the total platinum content in tumor tissue for some of the analyzed compounds. Consequently, we have demonstrated that LA-ICP-MS analysis is capable to determine platinum levels located specifically in the malignant parts of the tumor tissue, while microwave-assisted digestion generally pretends higher platinum concentrations, thus may cause misleading conclusions.

Platinum distribution in kidney sections using LA-ICP-MS

In addition to the tumor samples, also the platinum distribution in kidney was investigated. This is of interest for metal-based anticancer drugs, as cisplatin treatment (which is routinely employed in half of the standard oncological treatment regimens in clinics)[9] is frequently associated with nephrotoxicity (one out of three patients).[42] In order to better understand the mechanisms involved in cisplatin-induced nephrotoxicity, several LA-ICP-MS studies have already focused on platinum imaging in murine kidney sections upon treatment with cisplatin.[24-26,28] However, there are so far no LA-ICP-MS investigations on the renal distribution of other platinum-based drugs like e.g. oxaliplatin and satraplatin. This is especially of interest, as nephrotoxicity has not been observed as major adverse effect for these two compounds during preclinical evaluation and/or in treatment regimens in clinics.[8,43,44] Consequently, in order to assess whether the renal platinum distribution of oxaliplatin (9 mg/kg, i.v.) and satraplatin (40 mg/kg, p.o.) differed from the published data on cisplatin, platinum accumulation maps were obtained by LA-ICP-MS (Figure 4). The upper threshold in the color code bar was set to a platinum concentration of ~5.2 µg/g for oxaliplatin and ~4.2 µg/g for satraplatin. In general, both compounds exhibited 8- to 10-times higher platinum levels in the cortex and corticomedullarly region than in the medulla of the kidney. The higher platinum accumulation in these regions is in good correlation to the LA-ICP-MS studies in renal sections of cisplatin-treated rats and mice.[24-26,28] However, in contrast to the obvious signs of nephrotoxicity observed in the cisplatin samples,[24-26,28] no signs of cell damage such as tubular necrosis was observed in H&E-stained samples of the animals, tested in this study (Figure S7). Together with a recent report on mice treated with the clinically-tested ruthenium compound KP1339, where also no correlation between the ruthenium distribution in renal tissue and nephrotoxicity was found[28], this raises the question whether LA-ICP-MS is an appropriate tool for the indication of toxic kidney damage. More detailed knowledge on the structure and toxicity of the species (intact parent compound and/or

metabolites) present in renal tissue is required. Consequently, drawing conclusions on possible renal toxicity of platinum-based drug treatment solely based on the quantitative platinum accumulation pattern might not be appropriate. Thus, during preclinical evaluation the assessment of indicative blood serum parameters are still needed in order to estimate the nephrotoxic potential of investigational metal-based anticancer drug candidates.

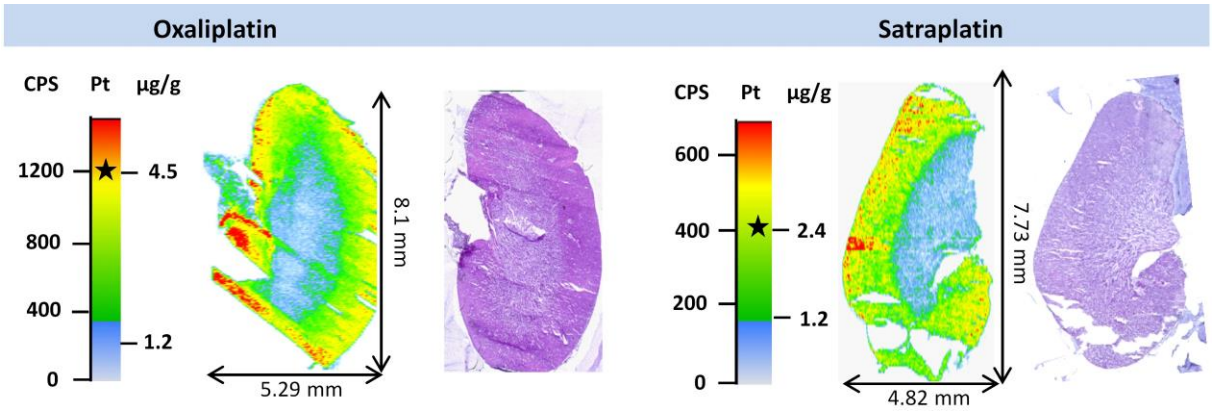

Figure 4. Distribution of platinum in kidney sections of CT-26-bearing mice treated either with oxaliplatin (9 mg/kg, i.v.) (left) or satraplatin (40 mg/kg, p.o.) (right). A consecutive H&E-stained cryosection is shown for comparison. The asterisks within the intensity bars correspond to the average platinum concentration determined by ICP-MS after microwave-assisted digestion.

Conclusions

A quantitative bioimaging method using LA-ICP-MS was successfully applied to tumor and kidney sections of CT-26-bearing mice upon treatment with platinum-based chemotherapeutics to compare spatially-resolved drug accumulation with histological structures. The platinum distribution maps of tumor samples (originating from six mice) obtained by LA-ICP-MS correlated with the histological pictures, which allowed discerning the platinum localization in cancerous and non-malignant tissue. Interestingly, (loose) soft tissue (e.g. connective tissue or microvessels) exhibited higher platinum contents than the malignant parts, especially for experimental compounds. Tumor heterogeneity observed histologically was reflected in the obtained platinum distributions as well. These information are lost in the case drug accumulation is studied solely by determination of total platinum tissue levels e.g. using ICP-MS analysis. Thus, histologically assigned quantitative data on drug uptake could contribute to a better understanding on the efficacy of metal-based antitumor compounds at an early preclinical stage. Therefore, knowledge on the spatially-resolved platinum distribution in tumor tissue could become an essential part in the lead compound selection for further anticancer drug development.

In addition, this study addressed the local platinum distribution in kidneys of treated animals. Oxaliplatin and satraplatin exhibited higher platinum levels in the cortex of kidneys than in the medulla, a pattern which was also observed previously in the case of cisplatin. Contrarily to cisplatin, the compounds included in our study have not shown to induce nephrotoxicity, to the best of our knowledge. This indicates that predictions on possible renal toxicity of platinum-based drug treatment solely based on the quantitative platinum accumulation pattern might not be appropriate.

Acknowledgements

We are thankful to G. Zeitler for animal care and Anita Brandstetter for support with the histological evaluations. We acknowledge Luca Bamonti for proof-reading this paper. This work was supported by the Austrian Science Fond grant P26603 (to P.H.). This work was performed in the surrounding of COST action CM1105.

References

1 L. R. Kelland, *Nat. Rev. Cancer*, 2007, **7**, 573-584.

2 T. W. Hambley, *Dalton Trans.*, 2007, 4929-4937.

3 M. Galanski, V. B. Arion, M. A. Jakupec and B. K. Keppler, *Curr. Pharm. Des.*, 2003, **9**, 2078-2089.

4 S. H. van Rijt and P. J. Sadler, *Drug Discov. Today*, 2009, **14**, 1089-1097.

5 D. Gibson, *Dalton Trans.*, 2009, 10681-10689.

6 E. Wexselblatt and D. Gibson, *J. Inorg. Biochem.*, 2012, **117**, 220-229.

7 M. D. Hall and T. W. Hambley, *Coord. Chem. Rev.*, 2002, **232**, 49-67.

8 H. Choy, C. Park and M. Yao, *Clin. Cancer Res.*, 2008, **14**, 1633-1638.

9 N. J. Wheate, S. Walker, G. E. Craig and R. Oun, *Dalton Trans.*, 2010, **39**, 8113-8127.

10 C. N. Sternberg, D. P. Petrylak, O. Sartor, J. A. Witjes, T. Demkow, J. M. Ferrero, J. C. Eymard, S. Falcon, F. Calabro, N. James, I. Bodrogi, P. Harper, M. Wirth, W. Berrry, M. E. Petrone, T. J. McKearn, M. Noursalehi, M. George and M. Rozencweig, *J. Clin. Oncol.*, 2009, **27**, 5431-5438.

11 M. V. S. Varma, Z. A. Radi, C. J. Rotter, J. Litchfield, A. F. El-Kattan and A. V. Lyubimov, in *Encyclopedia of Drug Metabolism and Interactions*, John Wiley & Sons, Inc., 2011.

12 G. C. Wallace, D. B. Ramsden and H. M. Grant, in *Encyclopedia of Drug Metabolism and Interactions*, John Wiley & Sons, Inc., Editon edn., 2012.

13 B. Gammelgaard, S. Stürup, C. Møller and A. V. Lyubimov, in *Encyclopedia of Drug Metabolism and Interactions*, John Wiley & Sons, Inc., 2011.

14 M. West, A. T. Ellis, P. J. Potts, C. Streli, C. Vanhoof, D. Wegrzynek and P. Wobrauschek, *Journal of Analytical Atomic Spectrometry*, 2012, **27**, 1603-1644.

15 J. S. Becker and N. Jakubowski, *Chem. Soc. Rev.*, 2009, **38**, 1969-1983.

16 J. S. Becker, M. Zoriy, A. Matusch, B. Wu, D. Salber, C. Palm and J. S. Becker, *Mass Spectrom. Rev.*, 2010, **29**, 156-175.

17 I. Konz, B. Fernández, M. Fernández, R. Pereiro and A. Sanz-Medel, *Anal. Bioanal. Chem.*, 2012, **403**, 2113-2125.

18 J. S. Becker, A. Matusch and B. Wu, *Anal. Chim. Acta*, 2014, **835**, 1-18.

19 D. Drescher, C. Giesen, H. Traub, U. Panne, J. Kneipp and N. Jakubowski, *Anal. Chem.*, 2012, **84**, 9684-9688.

20 C. Giesen, T. Mairinger, L. Khoury, L. Waentig, N. Jakubowski and U. Panne, *Anal. Chem.*, 2011, **83**, 8177-8183.

21 J. Seuma, J. Bunch, A. Cox, C. McLeod, J. Bell and C. Murray, *Proteomics*, 2008, **8**, 3775-3784.

22 E. Moreno-Gordaliza, D. Esteban-Fernandez, C. Giesen, K. Lehmann, A. Lazaro, A. Tejedor, C. Scheler, B. Canas, N. Jakubowski, M. W. Linscheid and M. M. Gomez-Gomez, *J. Anal. At. Spectrom.*, 2012, **27**, 1474-1483.

23 I. Khalaila, A. Bergamo, F. Bussy, G. Sava and P. J. Dyson, *Int. J. Oncol.*, 2006, **29**, 261-268.

24 M. Zoriy, A. Matusch, T. Spruss and J. S. Becker, *Int. J. Mass Spectrom.*, 2007, **260**, 102-106.

25 E. Moreno-Gordaliza, C. Giesen, A. Lázaro, D. Esteban-Fernández, B. Humanes, B. Cañas, U. Panne, A. Tejedor, N. Jakubowski and M. M. Gómez-Gómez, *Anal. Chem.*, 2011, **83**, 7933-7940.

26 O. Reifschneider, C. A. Wehe, I. Raj, j. Ehmcke, G. Ciarimboli, M. Sperling and U. Karst, *Metallomics*, 2013, **5**, 1440-1447.

27 D. Gholap, J. Verhulst, W. Ceelen and F. Vanhaecke, *Anal. Bioanal. Chem.*, 2012, **402**, 2121-2129.

28 A. E. Egger, S. Theiner, C. Kornauth, P. Heffeter, W. Berger, B. K. Keppler and C. Hartinger, *Metallomics*, 2014, **6**, 1616-1625.

29 J. Bianga, A. Bouslimani, N. Bec, F. Quenet, S. Mounicou, J. Szpunar, B. Bouyssiere, R. Lobinski and C. Larroque, *Metallomics*, 2014, **6**, 1382-1386.

30 S. Theiner, H. Varbanov, M. Galanksi, A. Egger, W. Berger, P. Heffeter and B. K. Keppler, *J. Biol. Inorg. Chem.*, 2015, **20**, 89-99.

31 H. P. Varbanov, S. Göschl, P. Heffeter, S. Theiner, A. Roller, F. Jensen, M. A. Jakupec, W. Berger, M. Galanski and B. K. Keppler, *J.Med.Chem.*, 2014, **57**, 6751-6764.

32 H. Varbanov, S. M. Valiahdi, A. A. Legin, M. A. Jakupec, A. Roller, M. Galanski and B. K. Keppler, *Eur. J. Med. Chem.*, 2011, **46**, 5456-5464.

33 H. P. Varbanov, S. M. Valiahdi, C. R. Kowol, M. A. Jakupec, M. Galanski and B. K. Keppler, *Dalton Trans.*, 2012, **41**, 14404-14415.

34 C. M. Giandomenico, M. J. Abrams, B. A. Murrer, J. F. Vollano, M. I. Rheinheimer, S. B. Wyer, G. E. Bossard and J. D. Higgins, *Inorg. Chem.*, 1995, **34**, 1015-1021.

35 L. Habala, M. Galanski, A. Yasemi, A. A. Nazarov, N. G. von Keyserlingk and B. K. Keppler, *Eur. J. Med. Chem.*, 2005, **40**, 1149-1155.

36 C. Paton, J. Hellstrom, B. Paul, J. Woodhead and J. Hergt, *J. Anal. At. Spectrom.*, 2011, **26**, 2508-2518.

37 http://www.iolite.org.au/Iolite.html.

38 http://imagej.nih.gov/ij/.

39 U. Jungwirth, D. N. Xanthos, J. Gojo, A. K. Bytzek, W. Koerner, P. Heffeter, S. Abramkin, M. A. Jakupec, C. G. Hartinger, U. Windberger, M. Galanksi, B. K. Keppler and W. Berger, *Mol. Pharamcol.*, 2012, **81**, 719-728.

40 R. Akhtar, S. Chandel, P. Sarotra and B. Medhi, *World J. Gastrointest. Oncol.* , 2014, **6**, 177-183.

41 G. Yothers, M. J. O'Connell, C. J. Allegra, J. P. Kuebler, L. H. Colangelo, N. J. Petrelli and N. Wolmark, *J. Clin. Oncol.*, 2011, **29**, 3768-3774.

42 X. Yao, K. Panichpisal, N. Kurtzman and N. Kenneth, *Am. J. Med. Sci.*, 2007, **334**, 115-124.

43 A. J. Armstrong and D. J. George, *Ther Clin Risk Manag.*, 2007, **3**, 877-883.

44 J. Cassidy and J.-L. Misset, *Semin. Oncol.* , 2002, **29**, 11-20.